08/30/2021

Geophysical investigations to determine the unknown extents of the abandoned Blackhawk gypsum mine, Blackhawk, SD

Phase 2

Prepared by:

Mohamed Khalil
Ph.D.

Former Assistant Professor
Geophysical Engineering Department
Montana Technological University
1300 West Park Street
Butte, MT 59701

Prepared for:

Fitzgerald Law Firm
343 Quincy Street; Ste 101
Rapid City, SD 57701

Table of Content

List of Figures

INTRODUCTION

The present report is the second phase-study of an integrated geophysical investigation to determine the unknown extent of the abandoned Blackhawk gypsum mine, SD. In the first phase (May 2021), the northern and northeastern parts were investigated. The findings of the first phase showed evidence of the extension of the abandoned gypsum mine in the southern part. Accordingly, the intention is made in this phase to do a complementary study investigating the southern and the western parts of the area. In this study, I used Electrical Resistivity Tomography (ERT) as the main method of exploration due to its high resolution, accuracy, and high data coverage. In total, twelve resistivity lines were measured using a Dipole-Dipole array. In addition, the Self-Potential method is used in some profiles, where no asphalt road exists, to detect water seepage. The Very Low-Frequency Electromagnetic method (VLF-EM) is used to show the approximate location of any subsurface conductive anomaly. The results of this phase of the study showed many subsurface abandoned mine tunnels in the southern part and some surface mining activities in the western part. The combination between the data of phase-1 and phase-2 went beyond my expectations. The distinction between the dry zone and the flooded zone is obviously clear, and the causes of the existence of 2016 and 2020 sinkholes have been explained. The expected locations of future sinkholes have been outlined.

METHEDOLOGY

ELECTRICAL RESISTIVITY TOMOGRAPHY (ERT)

Electrical Resistivity Tomography (ERT) is an active method that images subsurface bulk electrical resistivity, which provides information about changes in subsurface lithology and groundwater saturation. During electrolytic conduction, the current flow is associated with the movement of ions in groundwater, and resistivity measurements are dependent on the porosity, salinity concentration, and clay content especially within unconsolidated sediments.

Dipole-Dipole array was chosen for this survey due to its high horizontal and vertical resolution, high data coverage (2069 data point/section), and reasonable depth of penetration. I tried to gather high-quality data. This was done by:

(1) Pouring salt water around the electrodes to decrease the contact resistance,

(2) Stacking of data (to measure each data point two times minimum to 20 times maximum),

(3) Accepting data only with a Standard deviation less than 0.5%,

The technique used is called 2D Electric Resistivity Tomography (ERT). The ERT method is known for its versatility, with the ability to function in regions with high relief. ERT is based on a conventional four-electrode resistivity system, where electric current is injected via two current electrodes and the potential difference is measured between the two potential electrodes. Many different electrode arrays can be used for an ERT survey.

The resistivity data were collected using a Lippmann 4 Point Light Earth Resistivity Meter. All information about this system is available via www.L-GM.de. In the present survey, I used the active electrodes that were developed especially for the Lippmann 4 Point Light Earth Resistivity Meter. By default, each electrode chain consists of 20 electrodes at a 5-meter distance. The resistivity data were edited for bad data where bad data points were deleted before inversion.

The 2D and 3D resistivity data were inverted using RES2DINV and RES3DINV (Geotomo Software, www.geotomosoft.com). The inversion code is based on the smoothness-constrained least squares method. I used the L1 norm smoothness constrained optimization method. This is more commonly known as a blocky model inversion method or robust method. The robust inversion method is recommended if the subsurface resistivity has sharp boundaries. During the inversion, the cells of the finite element mesh were kept in their original value in some sections. In other sections, I used the half-width of the cell to enhance the inversion.

SELF-POTENTIAL (SP)

It is also known as spontaneous potential. It is a non-intrusive geophysical method that measures the electrical potential caused by subsurface current sources, such as fluid flow in porous media. Streaming potentials are pH-dependent and dominated by the electrical double-layer phenomenon as fluid flow through pore spaces causes an excess drag of the built-up positive charge on mineral grains, expressed as a streaming current density. In turn, the positive self-potentials are attributed to the direction of fluid flow, so that the negative self-potential indicates downward seepage.

We collected self-potential measurements for each resistivity line except those located on asphalt road, where no direct contact with the soil layer could be achieved. We used two saturated lead chloride non-polarizing electrodes with a high impedance voltmeter. The survey utilized the potential amplitude method with the reference electrode fixed at the base station, and the roving electrode moved progressively from station to station. This method allows for a small cumulative error in measurements as well as avoiding the confusion of polarity, allowing for a drift correction to be applied.

VERY LOW FREQUENCY ELECTROMAGNETIC (VLF-EM)

The theoretical basics of VLF-EM, in addition to its geological and hydrogeological applications, can be found in literature, e.g., McNeill and Labson (1991). A low-frequency field is sent out from many radio transmitters distributed in different parts of the world, designed for military communications and navigation. The transmitted frequency is usually between 15–30 kHz. At very large distances, these powerful radio transmitters induce electric currents in buried conductive structures. Induced currents produce secondary magnetic fields that can be detected at the surface through deviations of the normal VLF field. The resultant elliptically polarized electromagnetic field consists of two components of the same frequency but of different amplitudes out of phase with each other. The amplitude of the component, which is in-phase with the primary field, is the real or in-phase component while the other component, which is out-of-phase with the primary field, is the imaginary or out-of-phase or quadrature component.

Qualitative interpretation of VLF-EM data is based on filtering procedures. Fraser (1969) and Karous–Hjelt (Karous and Hjelt 1983) filtering are the two methods most widely used in processing VLF-EM data. Fraser filter is applied to the tilt angle of the magnetic polarization ellipse (real component). The Fraser filter calculates horizontal gradients and smoothes the data to give maximum values over conductors that can then be contoured. Fraser filter transforms the zero-crossing points into peaks, enhancing the signals of the conductive structures. The center of the anomalous structure may fall directly under the peak of the Fraser filtered data. Another effective filtering technique was proposed by Karous and Hjelt (1977, 1983). It generates an apparent current density pseudo-section by filtering the in-phase data. In general, higher values of relative current density correspond to the subsurface conductive anomaly, whereas lower values of relative current density correspond to higher values of resistivity (Benson et al. 1997).

RESULTS AND DISCUSSION

Figure (1) shows the location of the measured resistivity lines and the coincident VLF, SP data. These lines could be divided into three groups:

Group B consists of four lines, which are B1, B2, B3, and B4. They locate in the north-eastern part of the area. Each line is 150m in length. The red arrow indicates the direction of measuring and the beginning of each section (X=0). These lines have been measured to support the results obtained in phase-1 and to establish a 3D resistivity model in this area.

Group Y has five lines, which are Y1, Y2, Y4, Y5, and Y6. They have been measured in this survey (phase-2) to detect any subsurface indication of mining activity in this area. The lengths of these lines range from 240m in Y-1 to 120m in Y-6.

Group O-P consists of three lines O-1, O-2, and P-1, which locate in the south-western part.

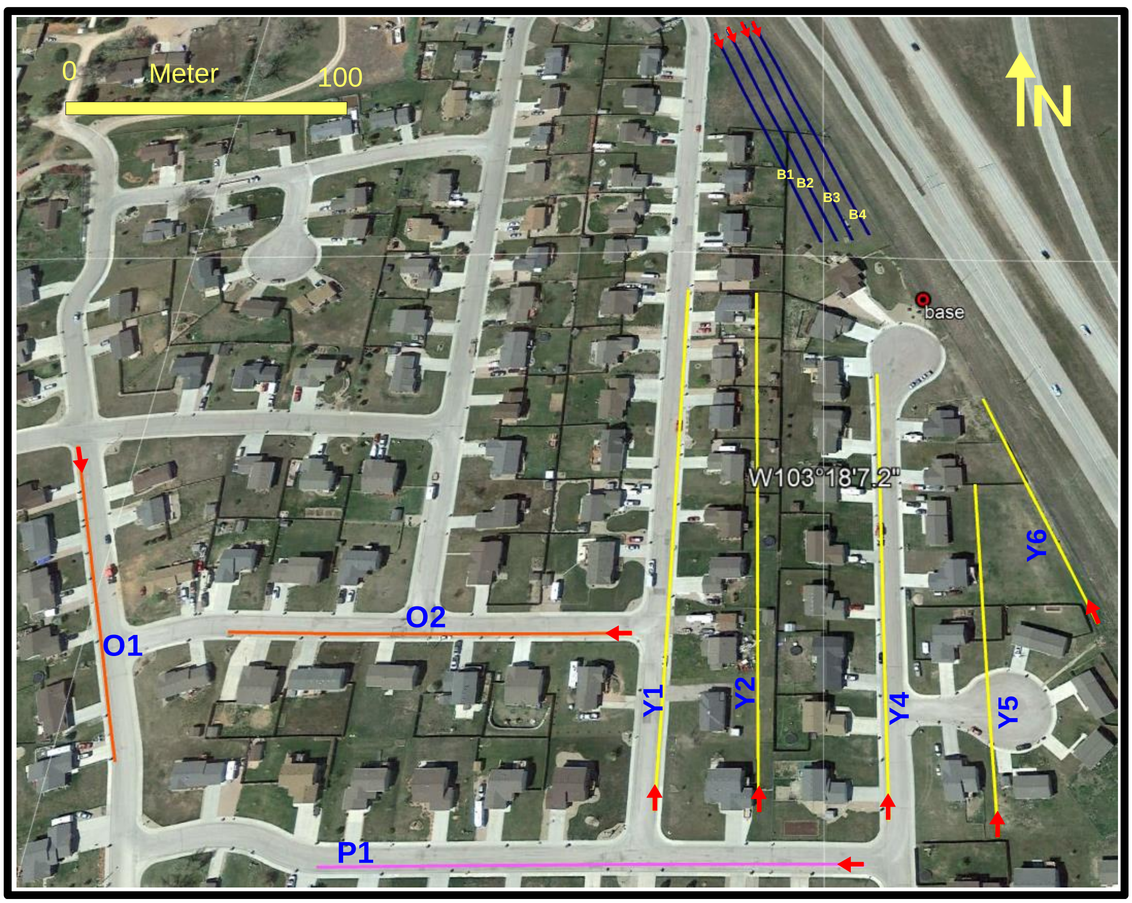

Fig. (1): Location map of the measured profiles.

Group-B

Lines B1, B2, B3, and B4 are shown in Figures 2,3,4, and 5 respectively. Resistivity Line-1 (Fig.2) shows low resistivity-tunnel shape anomalies located between 7.3 m to 14.5 m depth. The VLF-EM data shows multiple peaks in the Fraser filter (Fig.2, c) and high current density zones in the K-H filter (Fig.2, b), which is represented by brown to red color. From a theoretical perspective, these peaks and high current density zones, qualitatively, outline the approximate locations of the subsurface conductive zones. It is obviously clear that the low resistivity tunnel shapes (blue) are in good matching with high current density in the K-H filter and the peaks of Fraser filter in many locations such as 40m, 80m, and 140m from the start point of the section.

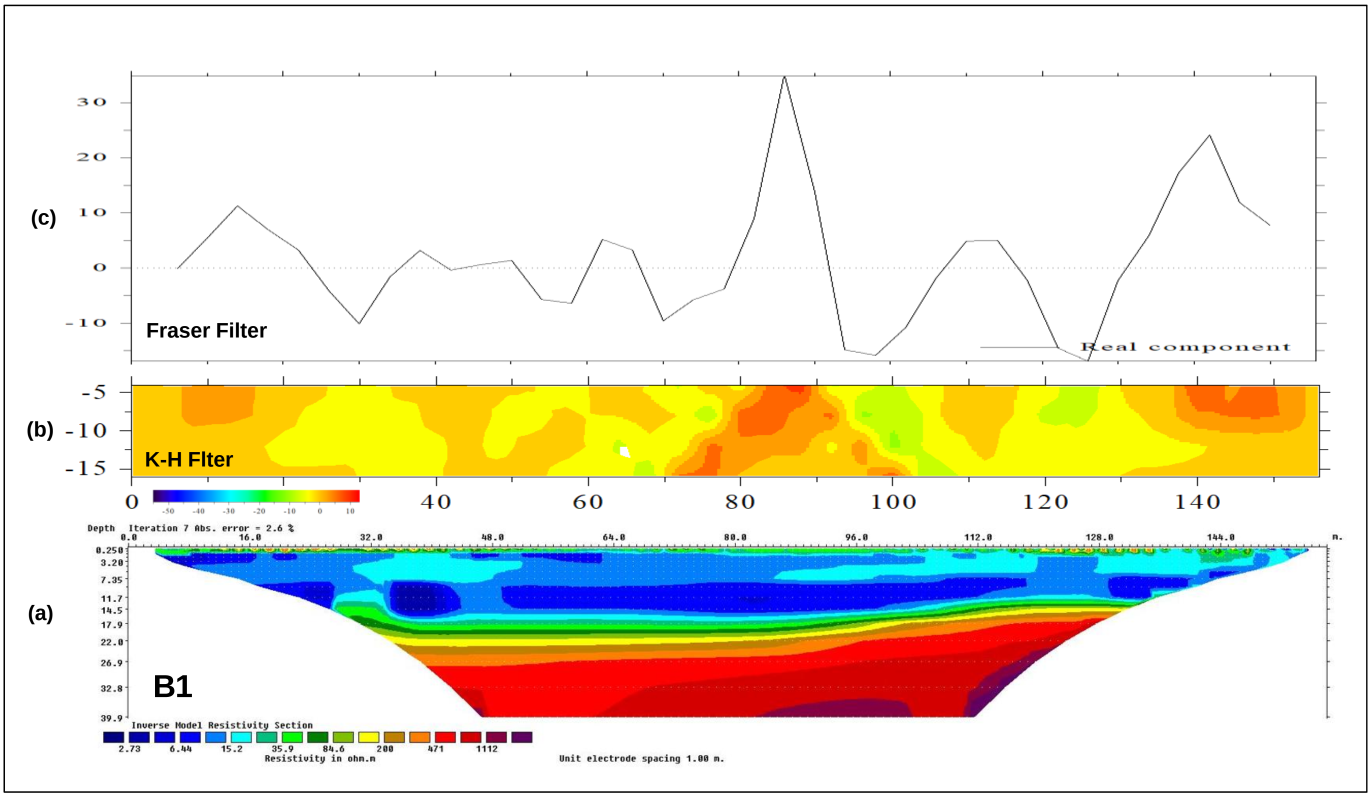

Fig. (2): ERT model of line B-1 (a), K-H filter of VLF-EM (b), and Fraser filter (c).

The same features could be observed in line B2 (Fig.3). The low resistivity tunnel-shape anomalies (blue color) at 20m, 40m, 80m, and 130m are associated with multiple peaks in the Fraser filter and high current density zones in the K-H-filter, particularly at 80m. In addition, Self-potential data has been collected for this line. It shows low magnitude SP values going to negativity and located very close to the aforementioned locations. The lower magnitude of SP in this survey may indicate a lower rate of seepage due to seasonal variation and higher saturation levels. It is worth noting that the two small anomalies located between 128m and 144m are two back-filled sinkholes located in a house backyard, as mentioned by the owner of this house.

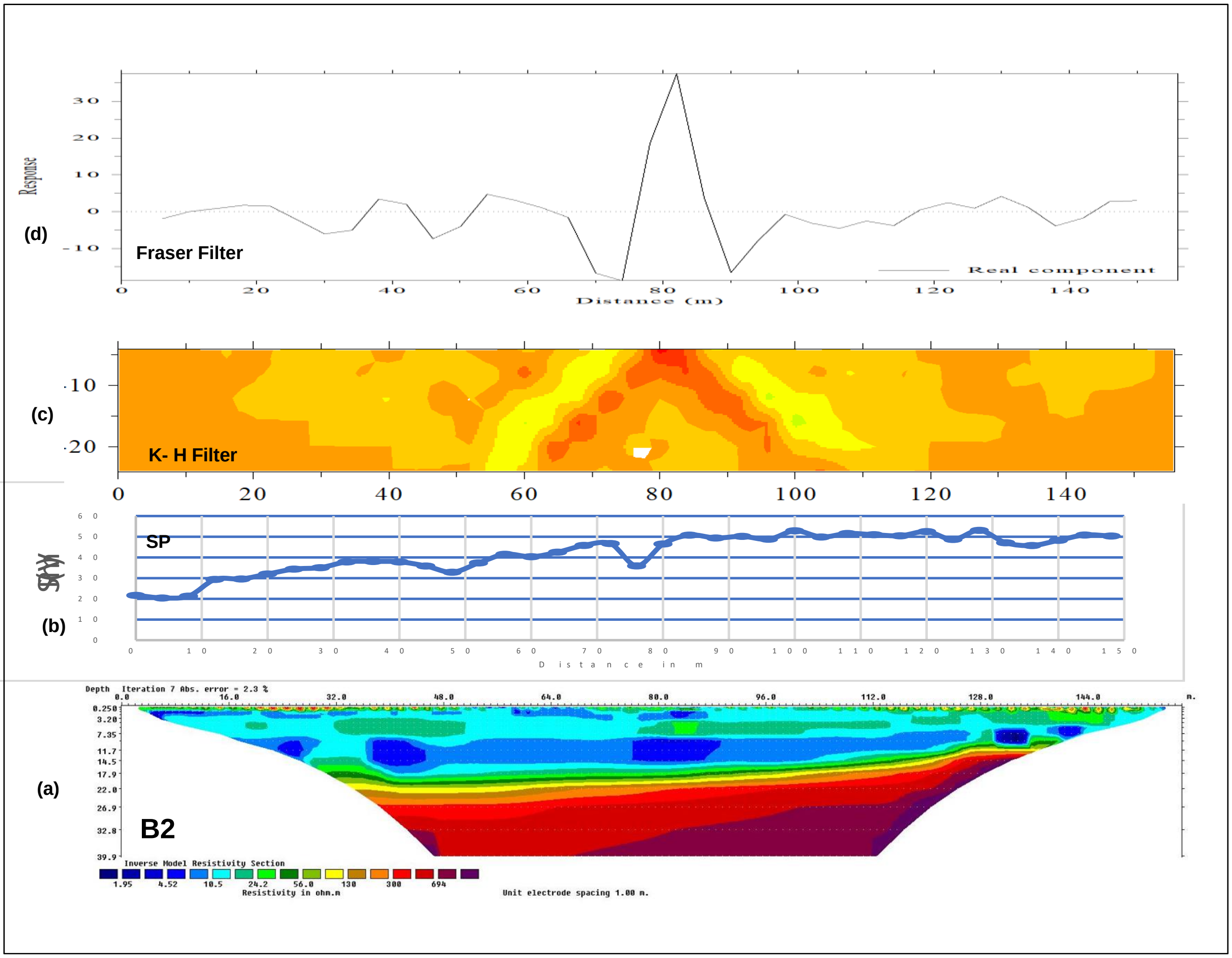

Fig. (3): ERT model of line B-2 (a), Self-Potential (b), K-H filter of VLF-EM (c), and Fraser filter (d).

Lines B3 and B4 (Figs.4 and 5) show approximately the same features and distribution of resistivity anomalies. The fence diagram (Fig.6) shows the resistivity distribution of lines B1, B2, B3, and B4. The continuity of subsurface low resistivity tunnel-shape anomalies is obvious in the east-west direction. Matching with tunnel-shape anomalies in P2 and P3 from Phase-1 of this study is clear also in Fig. (7).

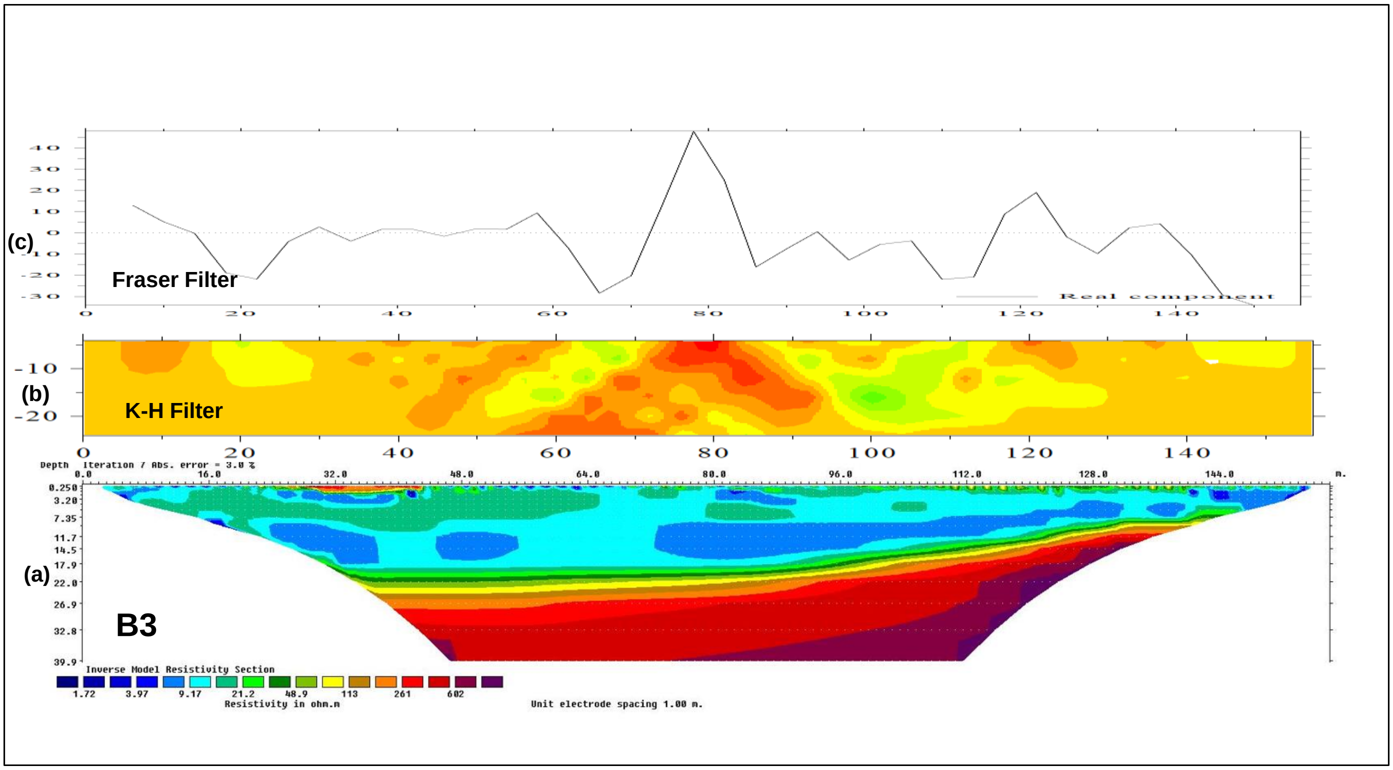

Fig. (4): ERT model of line B-3 (a), K-H filter of VLF-EM (b), and Fraser filter (c).

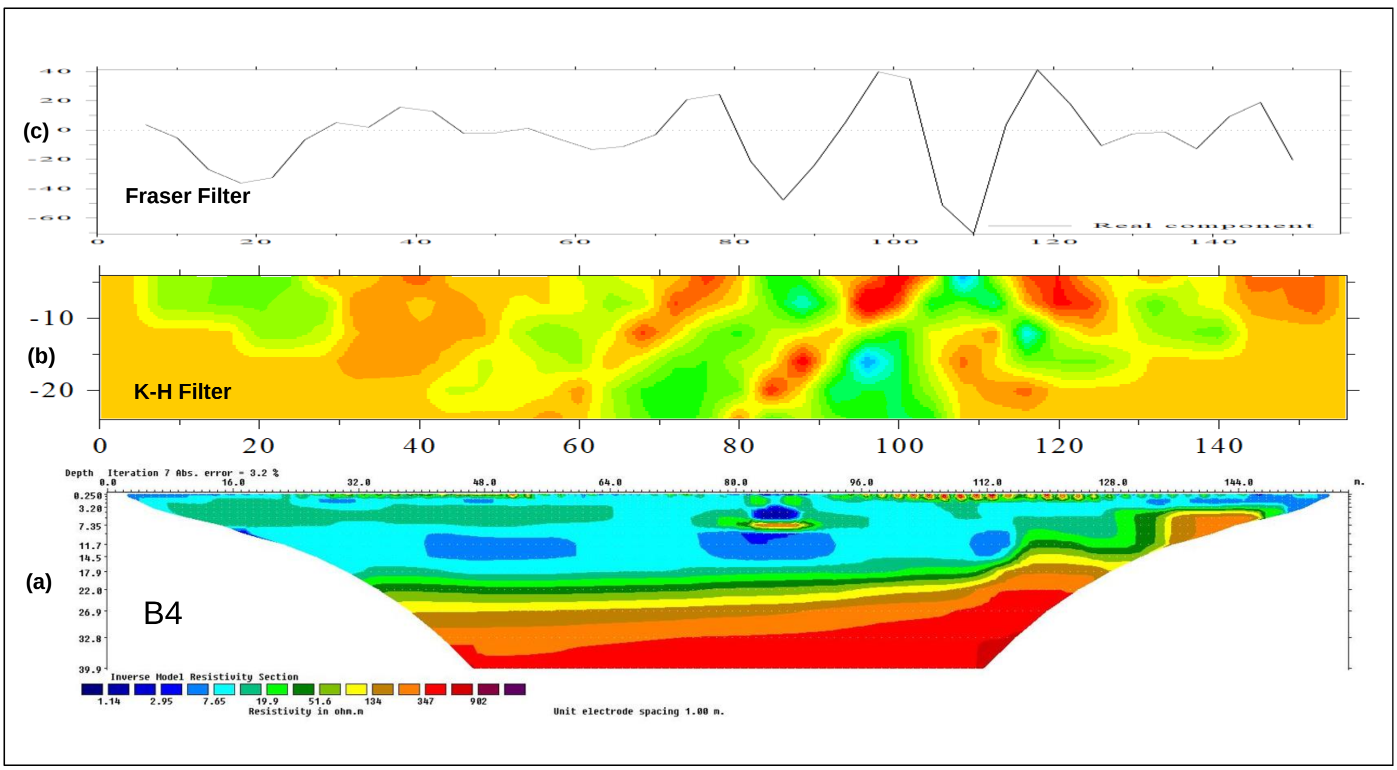

Fig. (5): ERT model of line B-4 (a), K-H filter of VLF-EM (b), and Fraser filter (c).

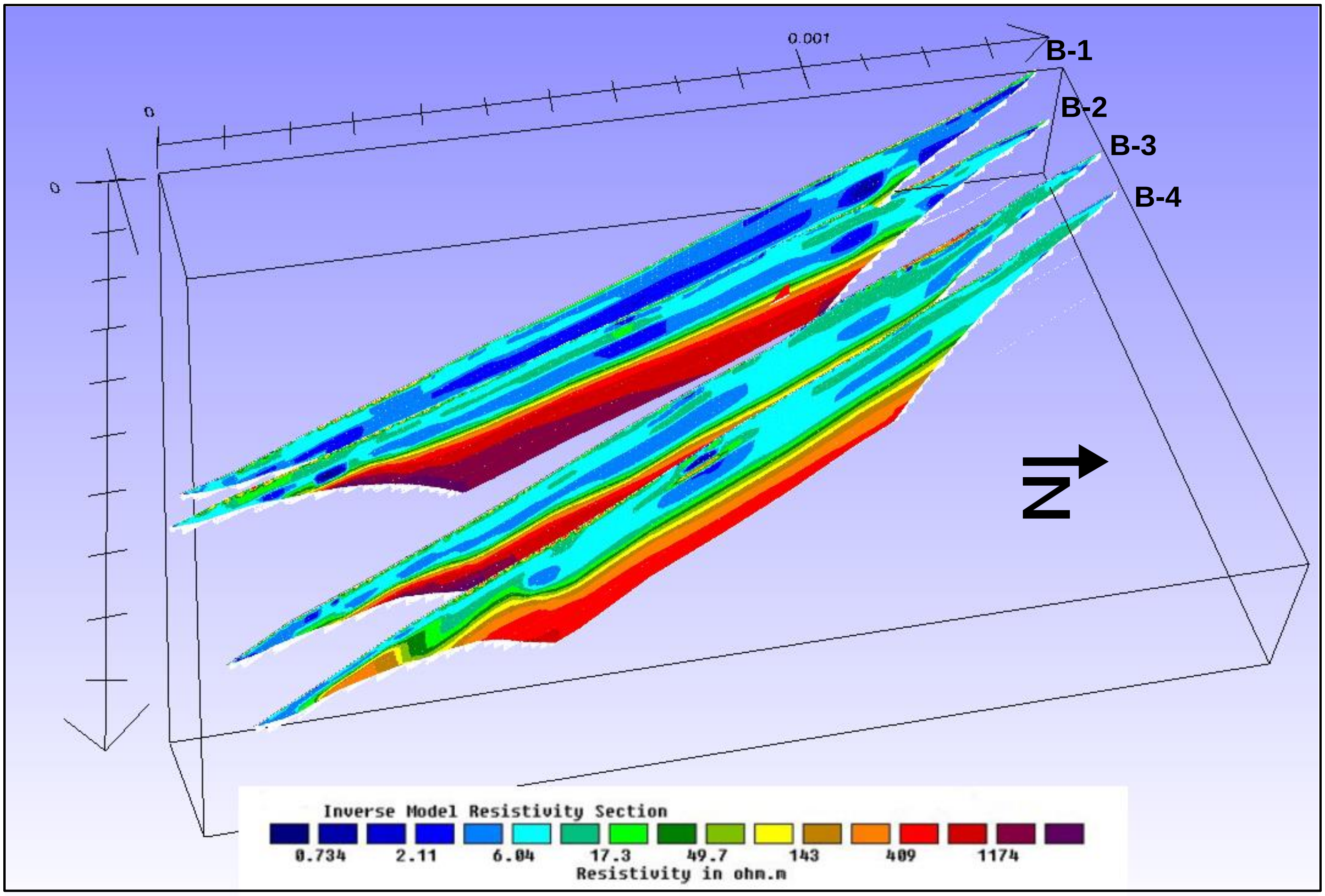

Fig. (6): Fence diagram of lines B1, B2, B3, and B4

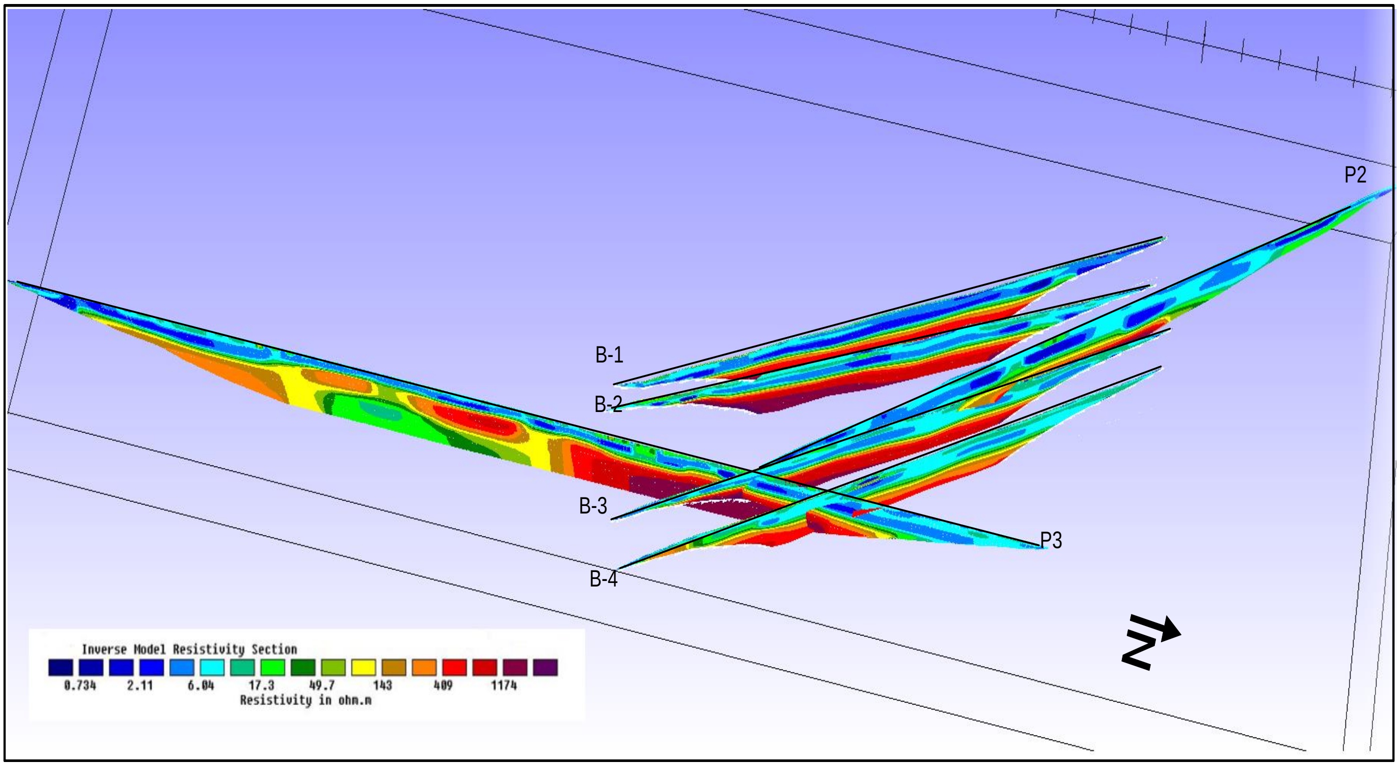

Fig. (7): Fence diagram showing lines of group B and lines P2 and P3 from phase 1.

Group Y

Figure (8) shows the 2-D resistivity model of line Y-1, extending 235 m in E Daisy Dr. The resistivity model (Fig.8, a) shows five high resistivity tunnel-shape anomalies extending from 5m to about 20 m depth. These anomalies are not associated with high current density or peaks of the K-H filter and Fraser filter, except the last anomaly at 192m, which supports the high resistivity nature of these anomalies. We could not measure SP to check any seepage because this line was on the asphalt road.

Figure (9) shows the 2-D resistivity model of line Y-2, which extends 235 m in the backyards (Fig.1). The resistivity model (Fig.9, a) shows five high resistivity anomalies at the same depth approximately, except the high resistivity anomaly at 144m is deeper than the other anomalies. These anomalies are not associated with high current density in the K-H filter or high peaks in the Fraser filter as well. SP data has been measured and shows a negative polarity above the first anomaly at 24 m, and the last two anomalies at 144m and 192m. The negative polarity of SP indicates a vertical seepage in these zones particularly in the northern side of the section, which is characterized by a lower topography.

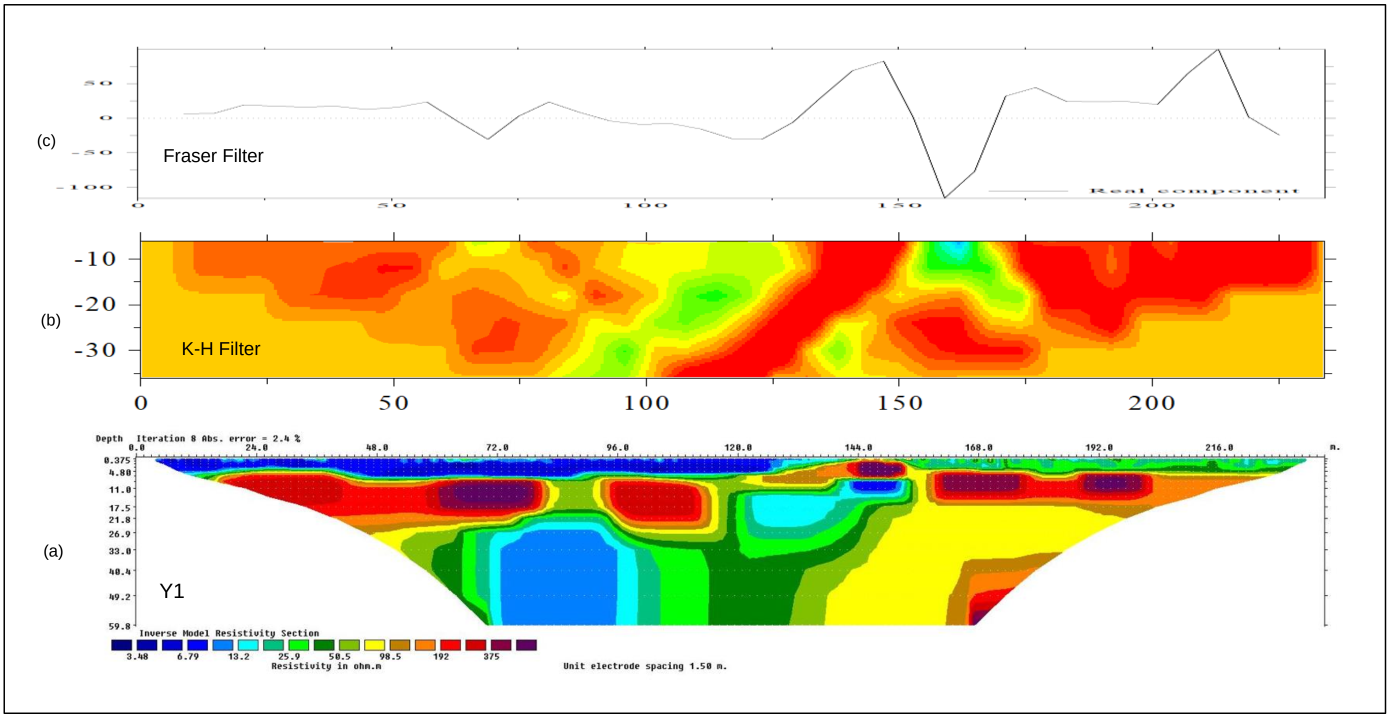

Fig. (8): ERT model of Line Y-1 (a), K-H filter of VLF-EM (b), and Fraser Filter (c).

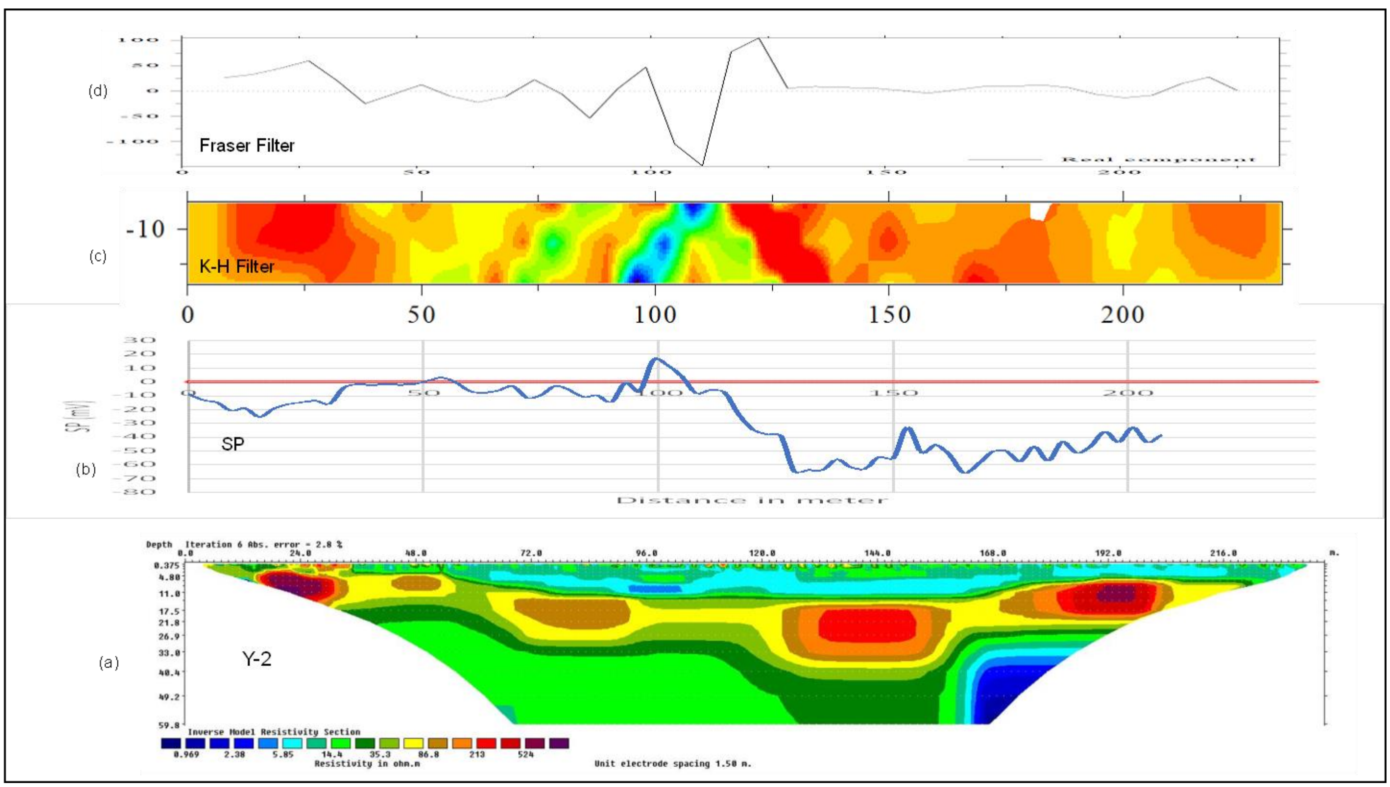

Fig. (9): ERT model of Line Y-2 (a), SP data (b), K-H filter of VLF-EM (c), and Fraser Filter (d).

Figure (10) shows the 2-D resistivity model of line Y-4, which extends 200 m in W. Elmwood Dr. (Fig.1). The resistivity model (Fig.10, a) shows two conductive tunnel-shape zones (dark blue). It also shows two small-scale sinkhole-shaped anomalies located between 15m and 20 m. The high conductive zones are associated with high current density in the K-H filter (Fig.10, b) and multiple peaks in the Fraser filter (Fig.10, c). Recently, American Engineering Testing (AET) has drilled six boreholes along this line as shown in Fig. (10, a). These boreholes are B2, B3, B4, B5, B6, and B7. The maximum depth of drilling is 51.5 feet (15.7 m) in B2 and B3, and 26.5 feet (8.1m) in B4, B5, B6, and B7. The subsurface geology varies between clay, shale, and gypsum of Sundance Formation. The majority of boreholes have a shallow depth and did not penetrate the expected tunnel shape anomalies. The groundwater level has been detected at 4.3 m in B3 and 3.2 m in B6, and no groundwater has been detected in the other boreholes. The discontinuity in groundwater level indicates a channeling system of flow along the west-east direction. Generally, detecting the groundwater in these boreholes indicates that this line and the next lines are saturated (flooded), which is reflected in low resistivity values. We could not measure SP because of the asphalt road. It is worth noting that, the resistivity of tunnel-shape zones has changed from high resistivity in lines Y-1 and Y-2, into low resistivity (conductive) in Y-4, which has a lower topography. This difference in resistivity could be attributed to water saturation. It is clearly obvious that the tunnel-shape anomalies of line Y-4 are fully saturated (flooded). This result is in good agreement with the results of phase-1, where resistivity sections located to the north of these sections (group B) are also completely flooded and the cavers could not continue the mapping of the mine. This difference in saturation may be the reason for the large number of land fractures that have been observed in the field between Y-2 and Y-4, where Y-3 is supposedly measured. We could not collect good data for Y-3 because a buried gas pipe along this line caused a large interference with the resistivity data. Another reason of bad quality data in this area is probably related to potential large-scale fractures that might open the electrical circuit between the resistivity meter and the ground.

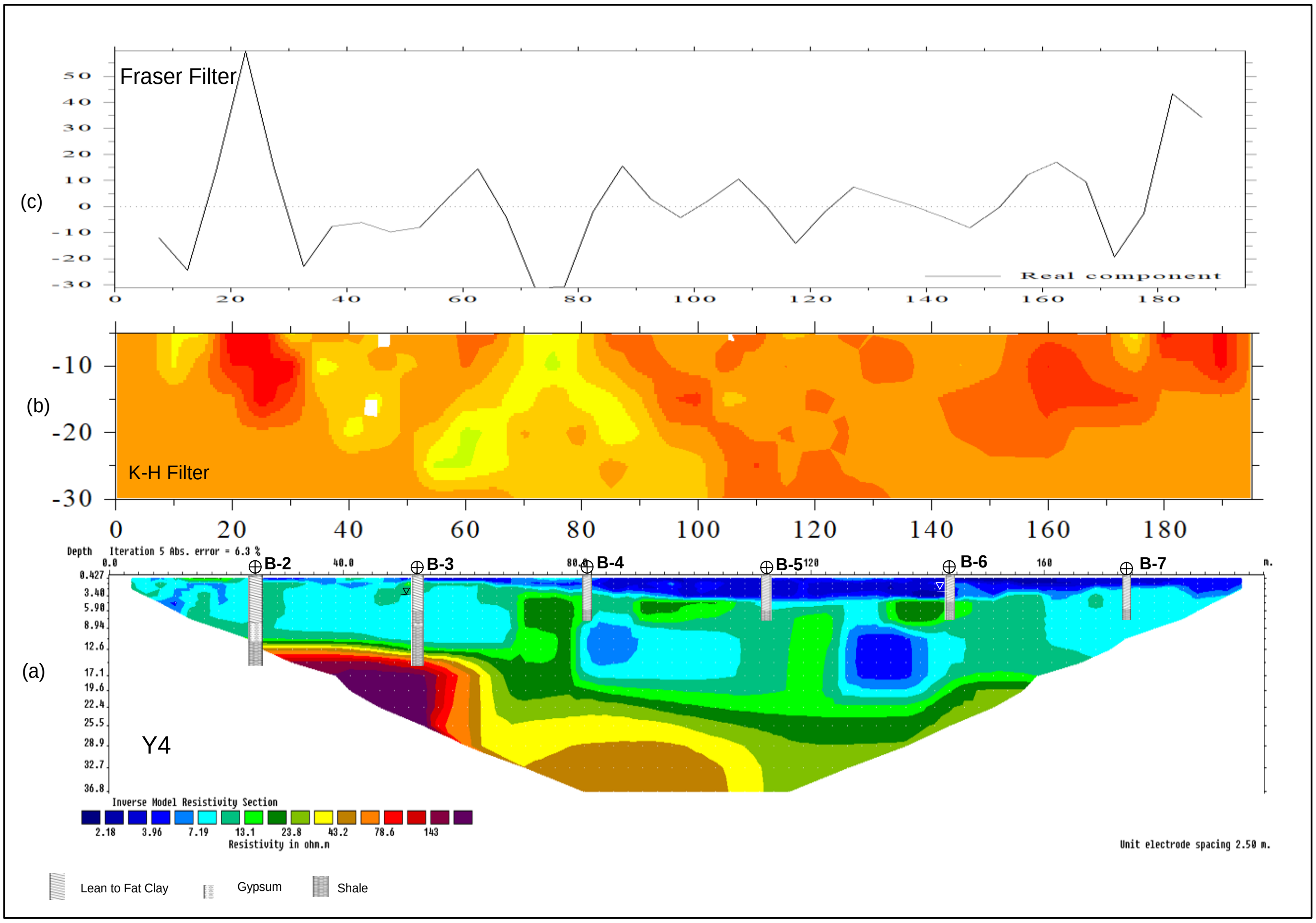

Fig. (10): ERT model of Line Y-4 (a), K-H filter of VLF-EM (b), and Fraser Filter (c).

Figure (11) shows the 2-D resistivity model of line Y-5, which extends 150 m, crossing the loop of Rainier Ct. (Fig.1). The resistivity model (Fig.11, a) shows a conductive tunnel-shape zone (dark blue) at 80m, but the resistivity is very low since the beginning of this line. It is associated with negative SP values (Fig.11, b), high current density in the K-H filter (Fig.11, c), and three obvious peaks in the Fraser filter (Fig 11, d). All these observations indicate high water saturation and water seepage downward. The direct contact of these high conductive tunnel -shape anomaly and the ground surface in some locations may indicate surface mining activities in the past. It is worth noting that the two small scale sinkhole-shape anomalies still exist in this profile also as an extension of the previous line (Y4). They are located between 25m and 35 m.

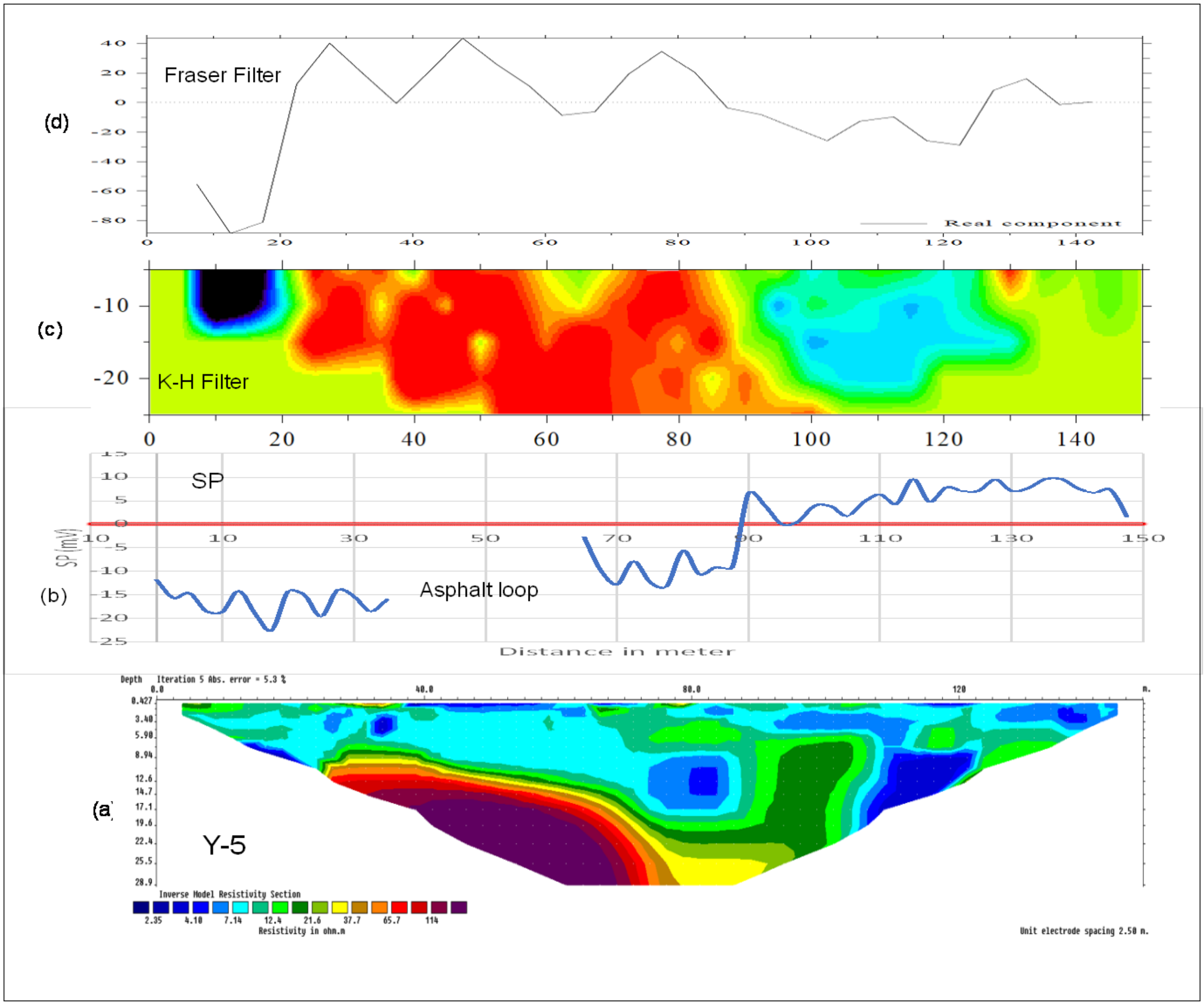

Fig. (11): ERT model of Line Y-5 (a), SP data (b), K-H filter of VLF-EM (c), and Fraser Filter (d).

Figure (12) shows the 2-D resistivity model of line Y-6, which extends 120 m, parallel to the high -way (Fig.1). The resistivity model (Fig.12, a) shows a highly conductive elongated zone (dark blue). This is because the line is not parallel to the previous lines. The high conductivity zone is associated with negative SP (Fig.12, b), high current density in the K-H filter (Fig.12, c), and three peaks in the Fraser filter (Fig.12, d). this line has the same saturation condition of the previous two lines Y4 and Y5. The present study shows that these lines Y4, Y5, and Y6 are completely flooded, the same as group B lines to the north.

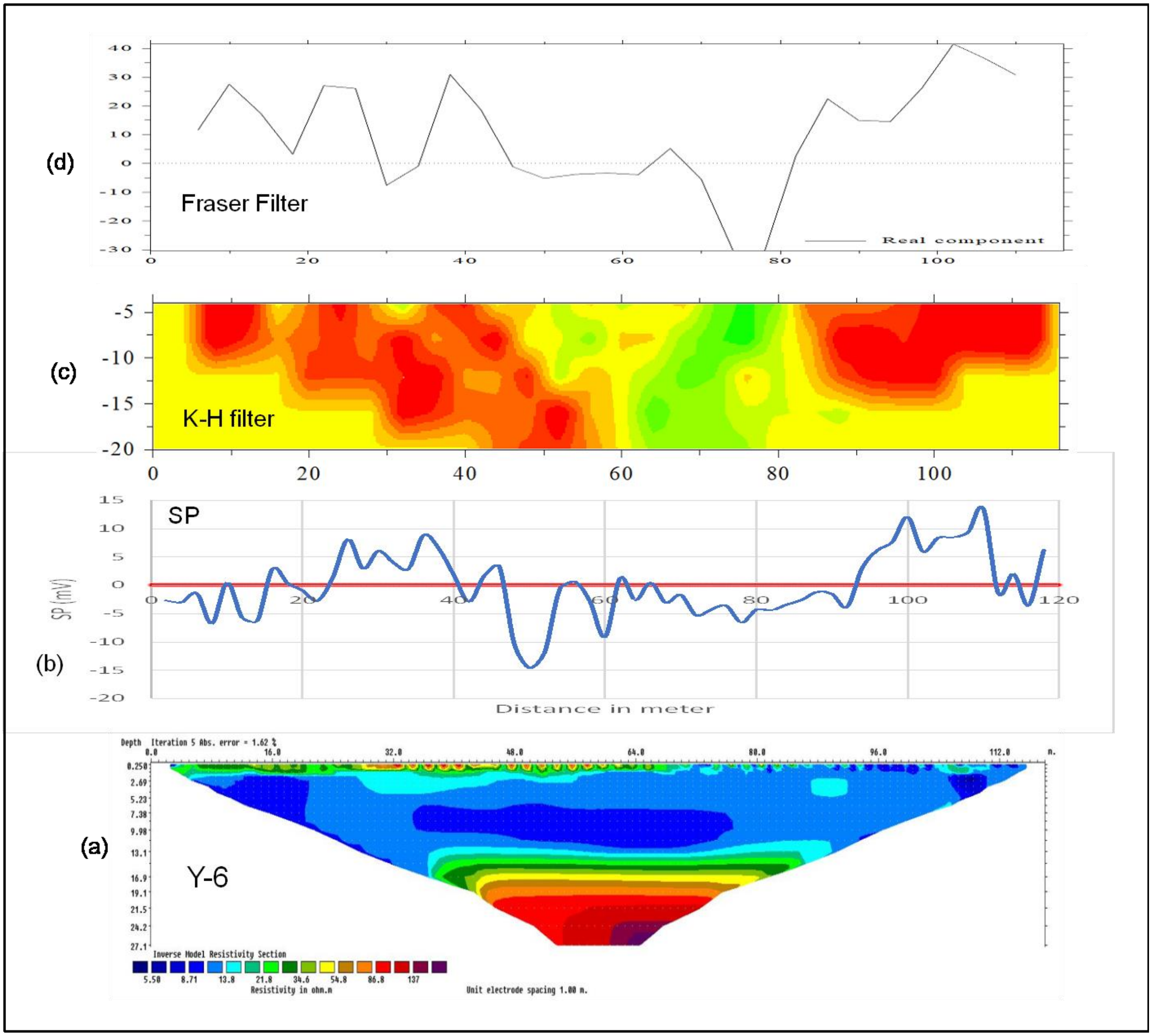

Fig. (12): ERT model of Line Y-6 (a), SP data (b), K-H filter of VLF-EM (c), and Fraser Filter (d).

Group O-P

Figure (13) shows the 2-D resistivity model of line O-1, which extends 150 m in Meadow Rose Ln (Fg.1). The resistivity model (Fig.13, a) shows two moderates to low resistivity tunnel-shape anomalies at 40m and 70m. The two anomalies are directly overlain by the conductive soil layer, which may refer to a surface mining at this location. The two anomalies are clearly represented in the K-H filter (Fig.13, b) by two high current density zones. They show two peaks in the Fraser filter as well (Fig. 13, c).

Figure (14) shows the 2-D resistivity model of line O-2, which extends 150 m in Blue Bell Dr. We could not measure SP data for this line and O-1 because all are measured in asphalt roads. VLF data of this line is very noisy because of the high cultural noise in this area. However, the resistivity model (Fig.14) shows a low resistivity depression extending from 40m to 80m. The depression is directly overlain by the soil layer which may refer to surface mining.

Figure (15) shows the 2-D resistivity model of lone P-1, which extends 200 m in Pengra Ln. We could not measure SP data for this line because of the asphalt road. VLF data of this line is very noisy as well because of high cultural noise. The resistivity model (Fig.15) shows two high resistivity zones at 70m and 120m (red color). Since this line is perpendicular to lines Y-1 and Y-2, these high resistivity zones seem to be the extension of the high resistivity tunnel-shape in lines Y-1 and Y-2.

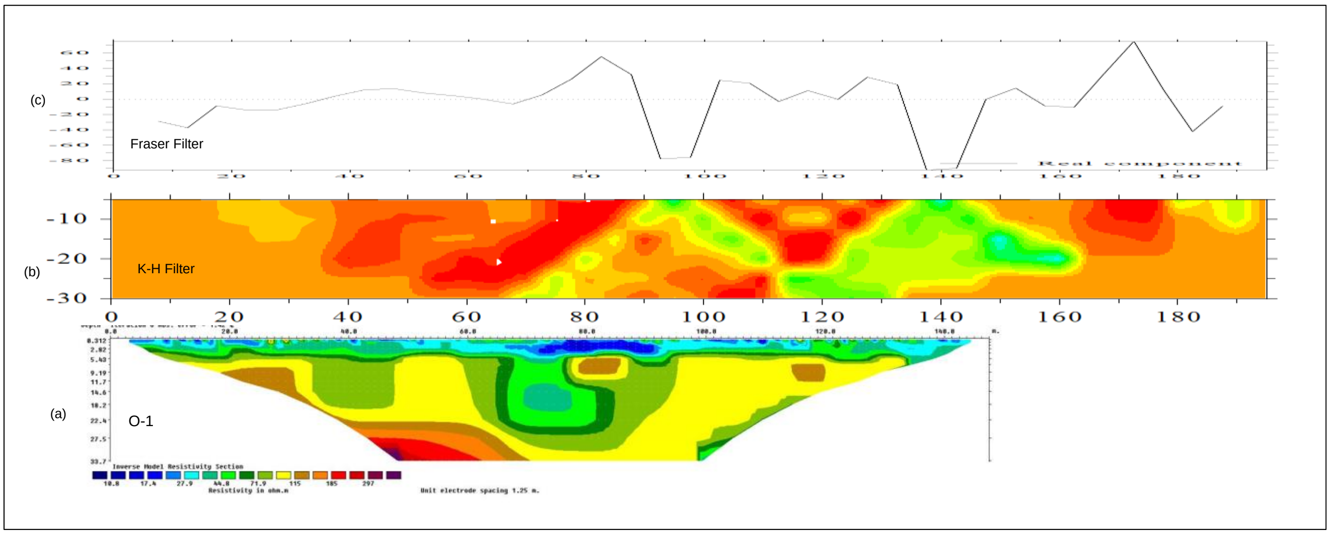

Fig (13): ERT model of Line O-1 (a), K-H filter of VLF-EM (b), and Fraser Filter (c).

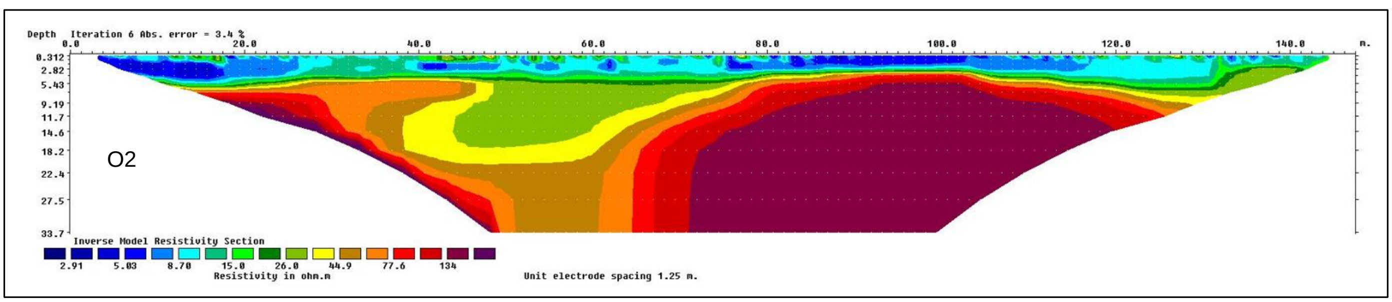

Fig (14): ERT model of Line O-2.

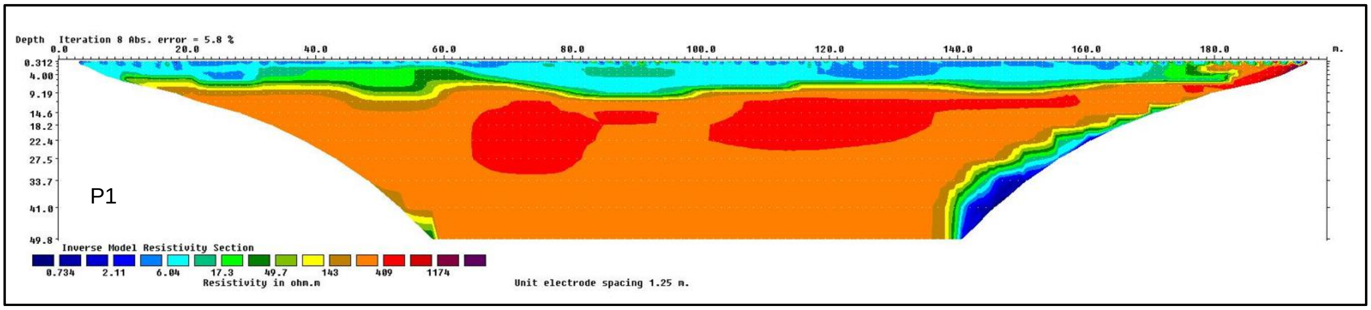

Fig (15): ERT model of Line P-1.

FENCE DIAGRAM

All 2-D resistivity lines which are measured in this study (phase-2) have been combined in the fence diagram (Fig.16). Each line has been plotted in its correct location and orientation. Examining Figure (16) shows that a considerable correlation between the tunnel-shape anomalies in the lines of group Y. lines Y1 and Y2 are characterized by high resistivity tunnel-shape anomalies, which could be interpreted as dry backfilling material or voids, that give favorable conditions for instability and creation of future sinkholes. Lines Y4, Y5, and Y6 are characterized by low resistivity tunnel-shape anomalies, which indicate that this area is flooded, the same as group B lines to the north. The area between lines Y2 and Y4 represents the transition zone from the dry layers above the groundwater table to the flooded layers below the groundwater table. This may explain the large number of surface fractures extending all along this area.

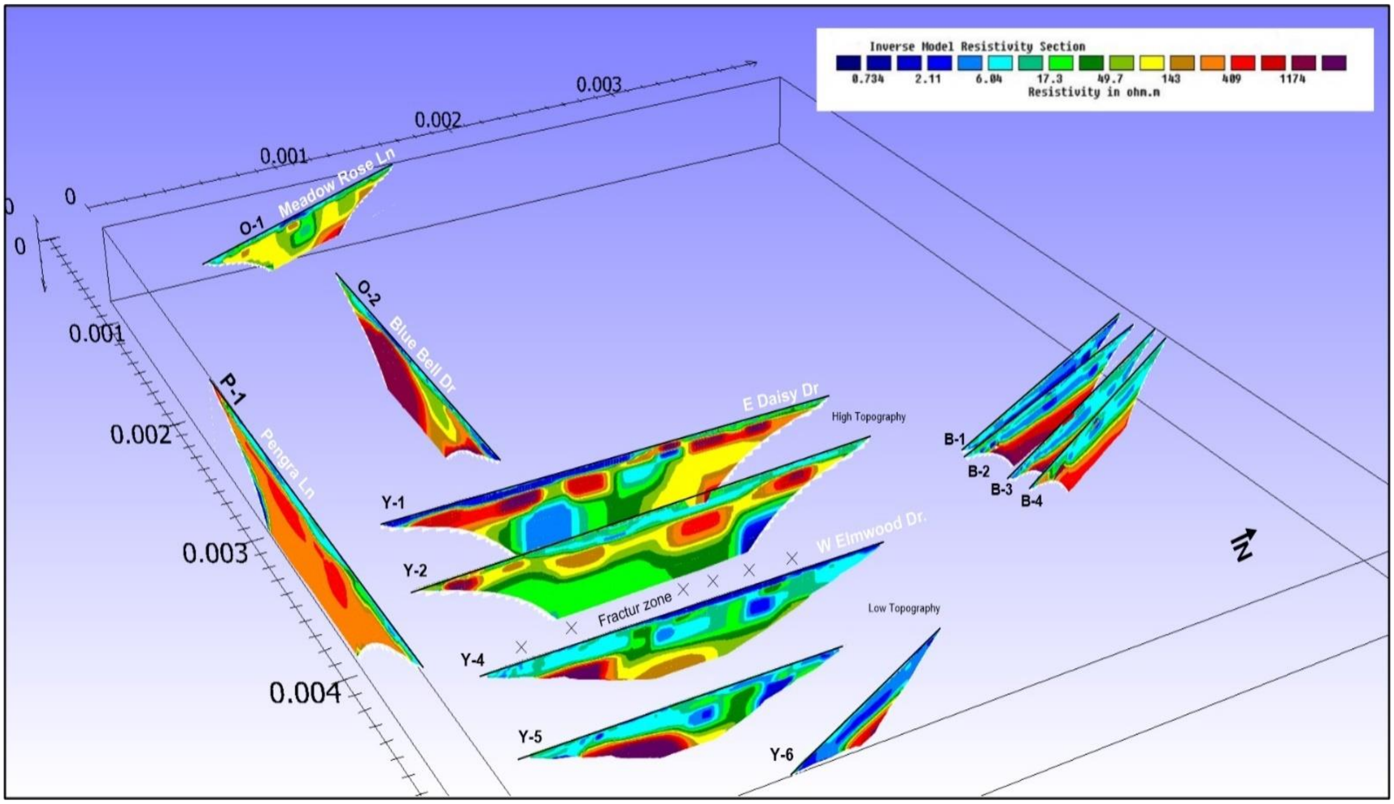

Fig. (16): Fence diagram combining the ERT models of all the lines

3-D RESISTIVITY MODELS

The 3D resistivity models of group B and group Y have been created in figures (17) and (18) respectively in the form of successive slice maps at different depths. Fig. (17) shows 15 maps from the ground surface, layer 1 (depth: 0.00-0.73 m) to layer 15 (depth: 28.4- 33.3 m). These maps show the details of resistivity distribution at each level. It is worth noting that layers 9, 10, 11, and 12 show the tunnel distribution in the area from 9.5 m to 20 m approximately. The layers below 20m level show the high resistivity layer that underlay the gypsum mine.

The 3D resistivity model of Group Y (Fig.18) shows 20 maps from the ground surface, layer 1 (depth: 0.00-0.5 m) to layer 20 (depth: 44.1-51.2 m). The first four layers until 2.5m depth show a large heterogeneity in the surface layer and a high resistivity zone to the northwestern zone. The high resistivity zone still exists in the next four layers until 6.8 m depth and clearly shows the resistive tunnel shape anomalies in Y1 and Y2. The next four layers from 6.8m to 14.5m clearly show the appearance of the conductive tunnels, which extend from the middle part of the map until the eastern side. The next four layers from 14.5 m to 28 m show the sharp contact between high resistive anomalies (dry) in the western part of the area (lines Y1 and Y2) and the conductive anomalies (flooded) in the eastern part (lines Y4, Y5, and Y6). This contact transgresses gradually to the east as the maps go deeper. These layers particularly show a good correlation between some dry tunnel shape anomalies in the west and flooded tunnels in the east. The last four layers from 28 m to 51 m show the resistive layer that underlay the mine. These layers usually have low resolution, where resolution of resistivity inversion usually decreases with depth.

.

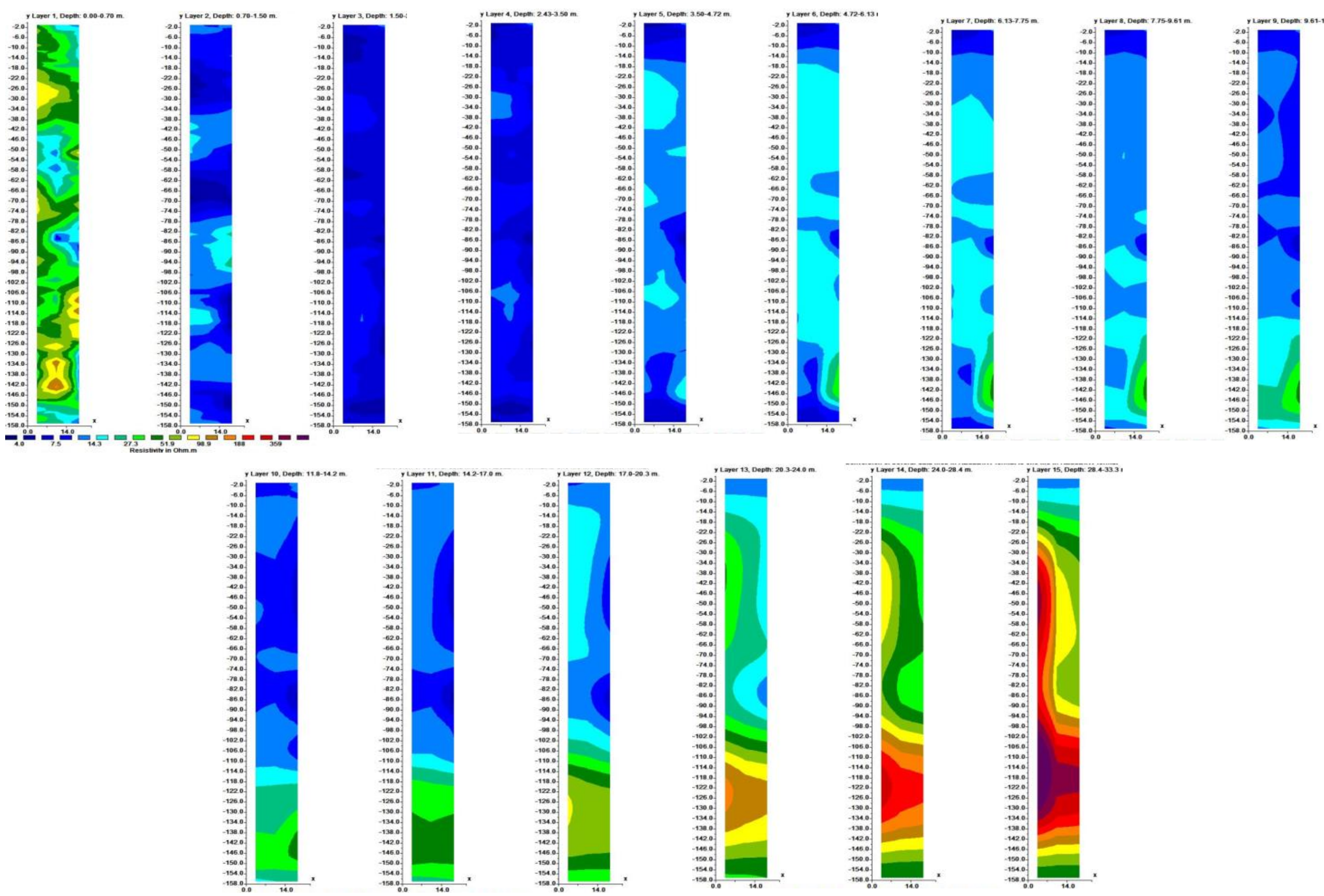

Fig. (17): 3D resistivity model of lines of group B.

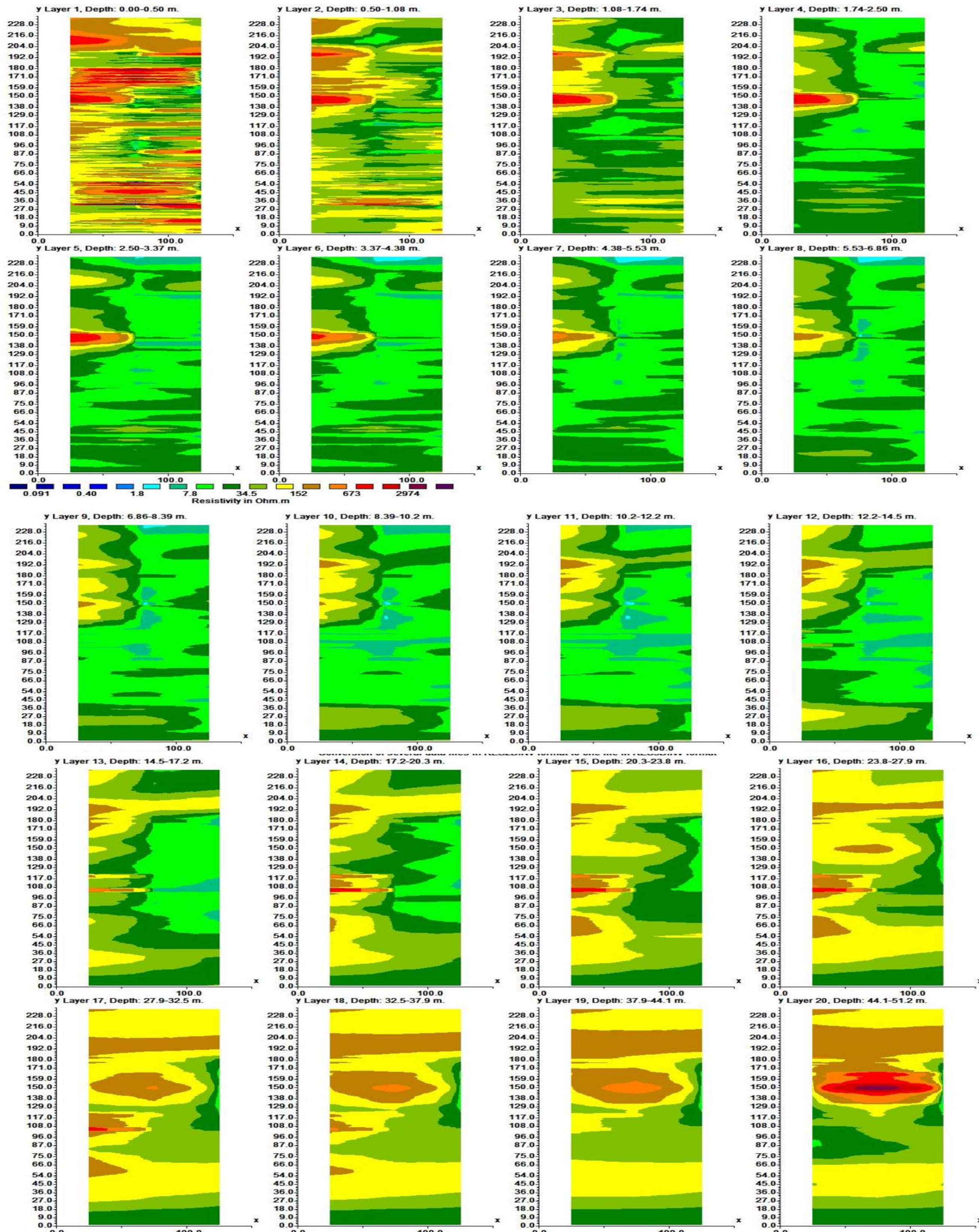

Fig. (18): 3D resistivity model of lines of group Y.

CONCLUSION

In figure (19), I tried to collect all resistivity lines that have been measured in phases 1 and 2 in the same fence diagram. In addition, the two sinkholes of 2016 and 2020 were plotted in their approximate locations. The target is to have a more detailed and integrated image of subsurface conditions of the area, that we must be cognizant. In fact, the area could be divided into two distinct zones.

1) The western area that has lines Y1, Y2, O-1, O-2, and P-1 from phase 2, lines P1, P7, P9, the western parts of P5 and P6, and the southern part of P3 from phase1. This part is generally characterized by high resistivity unsaturated layers. It has high resistivity tunnel-shape anomalies in some sections (Y1, Y2, P1, P5, and P7), a proposed surface mining in some sections (O-1, O-2), and no characteristic features could be observed in others (P-1 and P9).

2) The eastern area that has resistivity lines Y4, Y5, Y6, B-1, B-2, B-3, and B-4 from phase-2 and lines P2, the eastern parts of P5 and P6, and the northern part of P3 from phase1. This part of the study area is characterized by conductive (low resistivity) tunnel-shape anomalies. As mentioned in phase1 and as it appears in this study, all these sections in the eastern part are flooded with groundwater. In addition, this zone has a lower topography than the western zone.

A proposed transition zone (dashed blue line in the diagram) could be plotted between these two aforementioned areas. It separates the upper western dry zone from the lower eastern flooded zone. This distinction is obviously clear in lines P5, P6, and P8. This line is passing through the approximate locations of the sinkholes of 2016 and 2020. It crosses the area between lines Y2 and Y4, which has many surface fractures (Fig. 20). It is most likely that this line represents the intersection between the water table and the gypsum layer, which is dipping to the east.

It is worth noting also, this line (dry zone-flooded zone transition) is in perfect matching with the sinkhole impact area (Fig.21).

My interpretation of these sinkholes is that the seasonal fluctuation of groundwater table (summer-winter regression and transgression cycles) for tens of years along this transition zone led to multiple successive cycles of saturation and desaturation of the overlying shale layers. This could cause an erosion of the lower part of shale in the short term or successive cycles of swelling and shrinking of shale in the long run. Any of these mechanisms is a favorable condition to create a collapse (sinkhole) at any weak spot. Accordingly, the fracture zone between Y2 and Y4 is the most favorable zone to have a sinkhole (s) in the future.

The hazardous area classification map (Fig.22) shows three categories of risks: high, medium, and low. This classification is based on heterogeneity of subsurface geomaterial resistivities, surface observation (fractures), and groundwater surface.

Matching between Interpretive exhibit of different classes of risk map (Fig.24) and the regulated mining map near Black Hawk Sinkhole from 1985 to 2020 (Fig. 25) shows a good matching between the sinkhole impact area and historic surface damage (red and blue polygons) in Fig. (25) and the high-risk zone (red area) in fig. (24). Another good matching also could be observed between the surface mining area (yellow hachured polygon) and the low-risk zone in Figure (24) that is characterized by surface mining activities shown in lines O-1, O-2, and P-1.

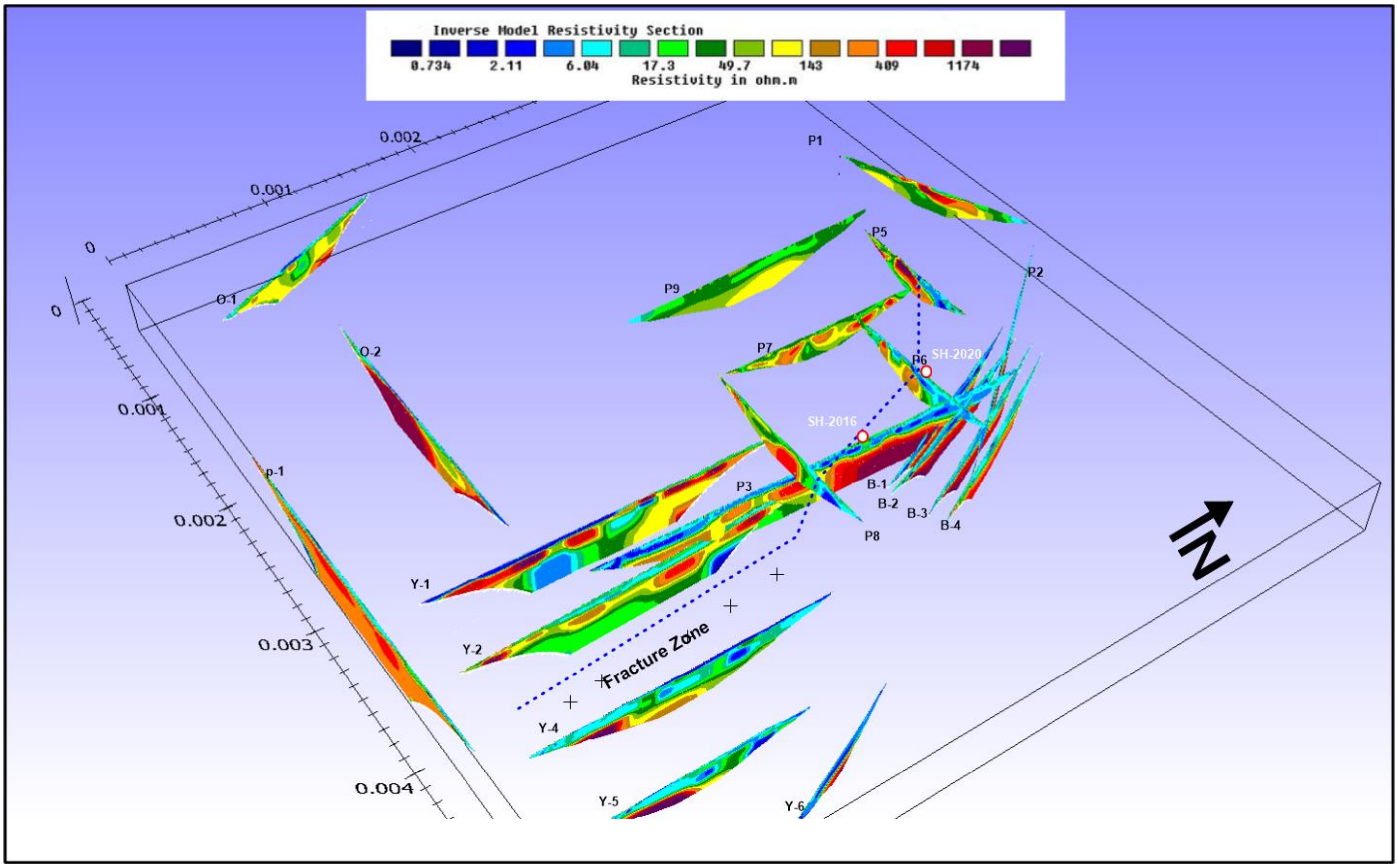

Fig (19): Fence diagram of all resistivity lines measured in phase1 and 2.

Fig (20): Surface fractures distributing between Y2 and Y4.

Fig (21): A map showing the sinkhole impact area.

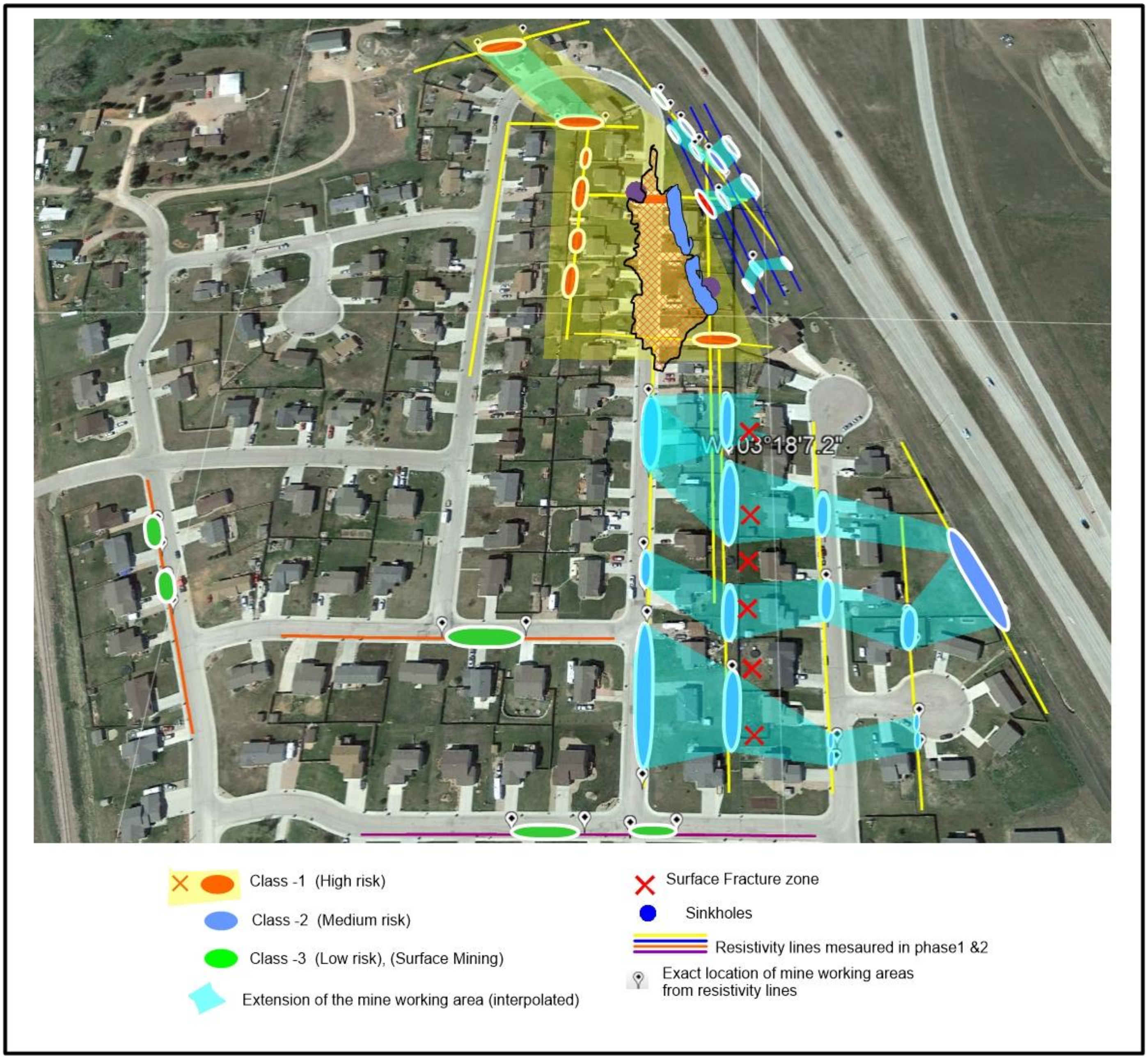

Fig. (22): Hazardous area classification and interpolated mine working areas extension.

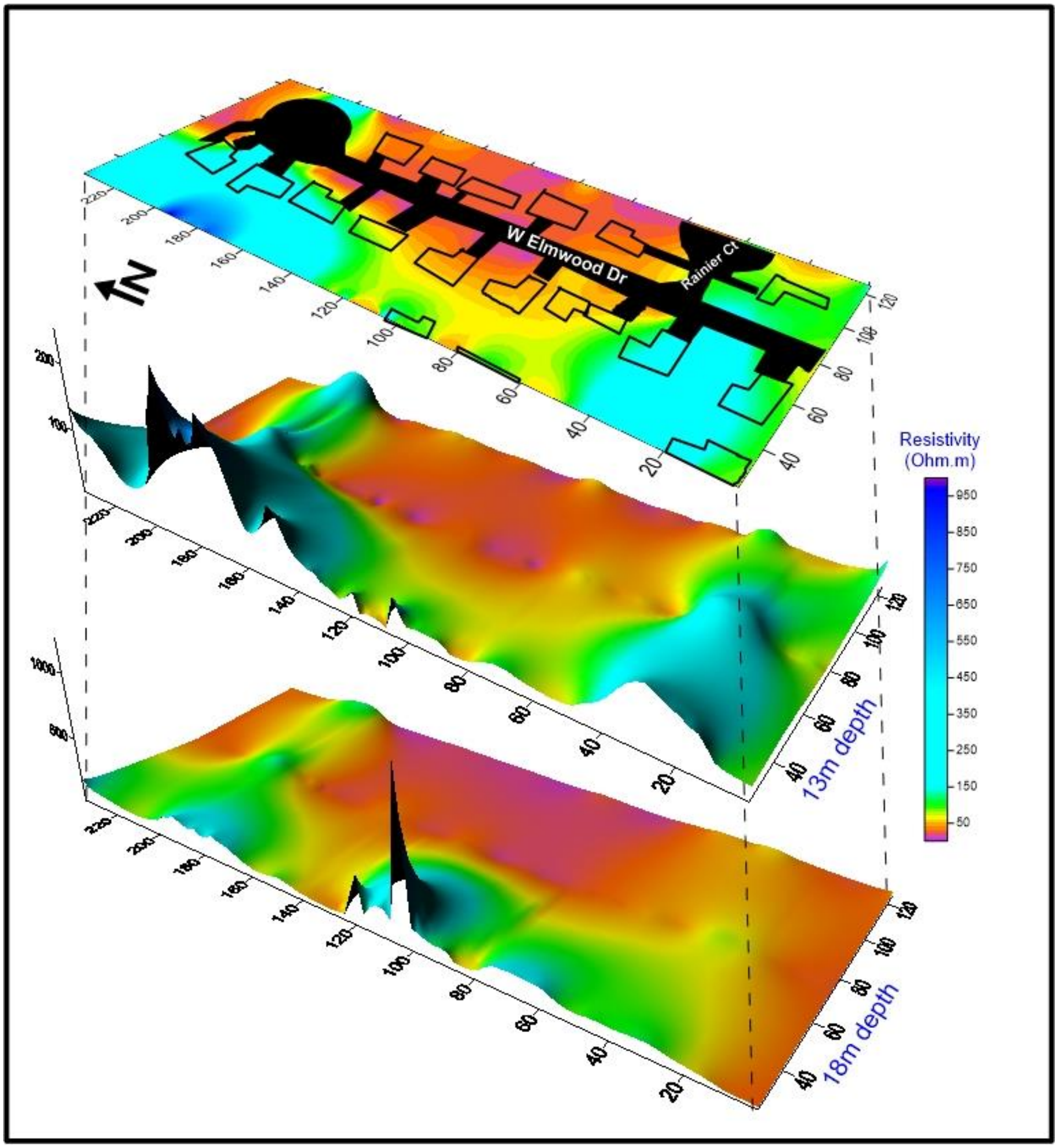

Fig. (23): Matching between the resistivity maps at 13 m and 18 m depth and the residential zone.

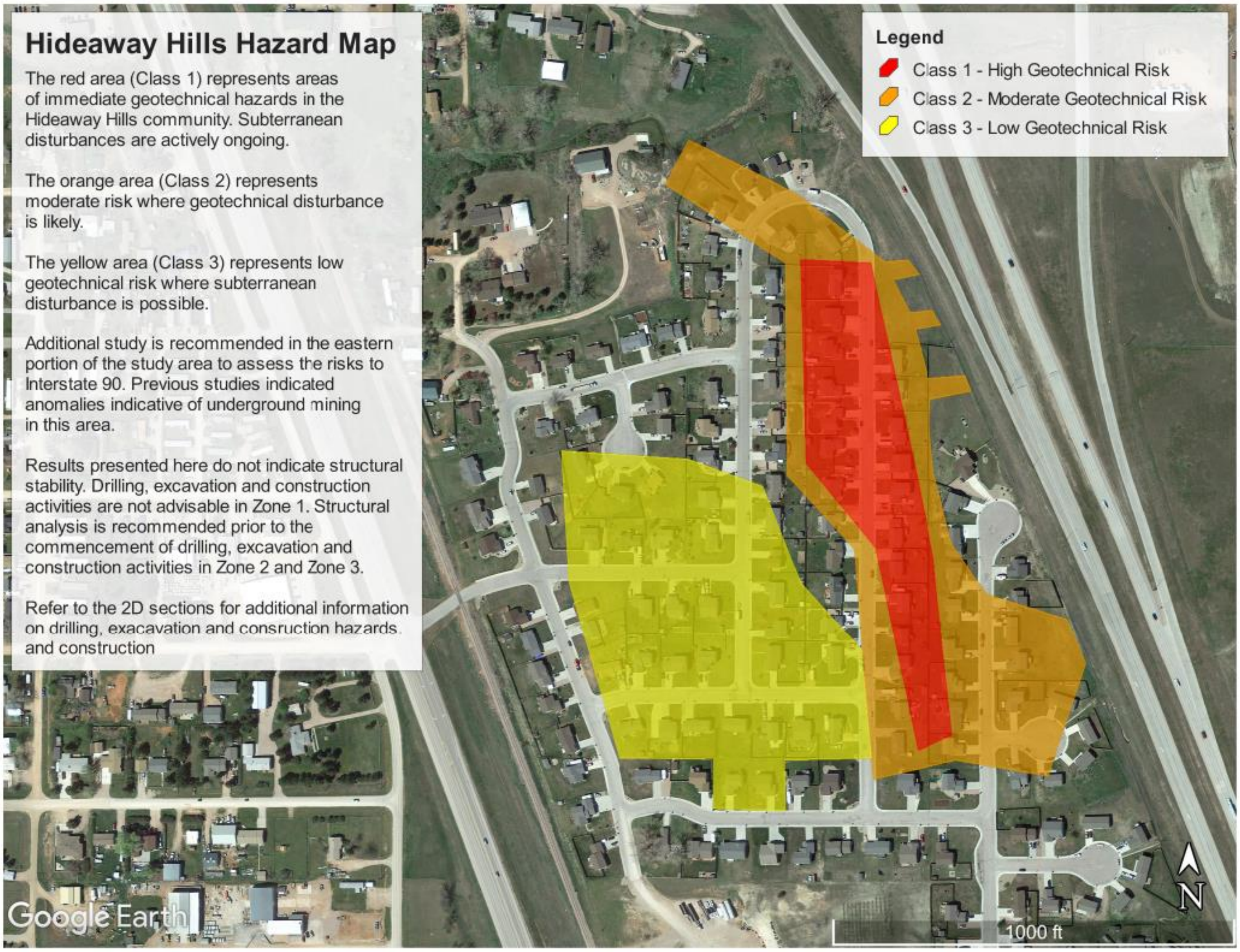

Fig. (24): Interpretive exhibit of different classes of risk.

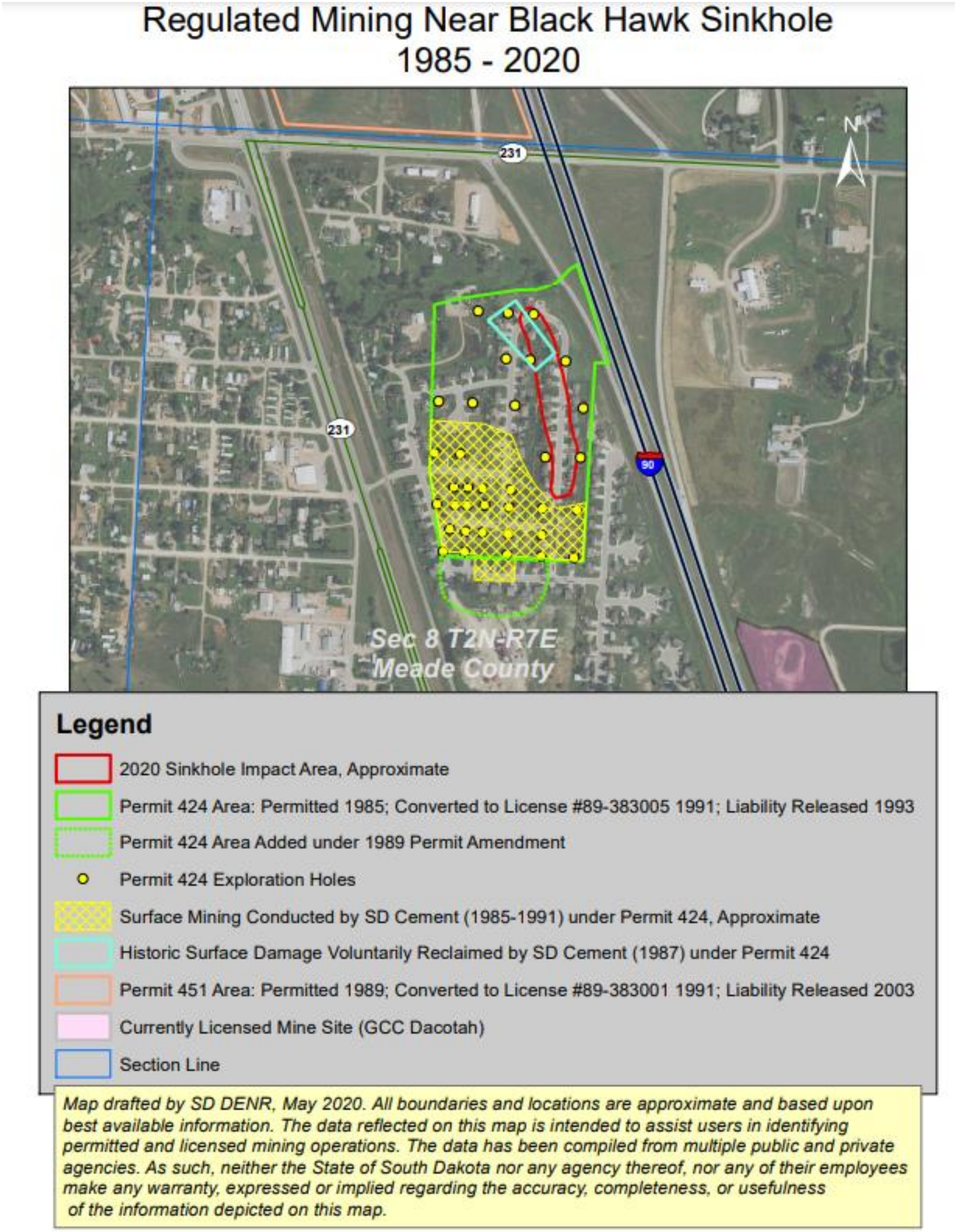

Fig. (25): Regulated mining near Black Hawk Sinkhole from 1985 to 2020.

REFERENCES

Benson A.K., Payne K.L. and Stubben M.A. 1997. Mapping groundwater contamination using dc resistivity and VLF geophysical methods – A case study. *Geophysics* **62**, 80–86.

Fraser D.C. 1969. Contouring of VLF-EM data. *Geophysics* **34**, 958–967.

Geonics, 2019. http://www.geonics.com/html/em31-mk2.html.

Karous M. and Hjelt S.E. 1977. Determination of apparent current density from VLF measurements. Report, Department of Geophysics, University of Oulu, Finland, Contribution no. 89.

Karous M. and Hjelt S.E. 1983. Linear filtering of VLF dip-angle measurements. *Geophysical Prospecting* **31**, 782–794.

Loke MH. Rapid 2D Resistivity & IP Inversion using the least-squares method: in Geotomo Software Manual. 1996.

Loke MH. Tutorial: 2-D and 3-D Electrical Imaging Surveys. Geotomo Software, Res2dinv 3.5 Software. 2004.

Martínez-Moreno FJ, Galindo-Zaldívar J, Pedrera A, González-Castillo L, Ruano P, Calaforra JM, et al. Detecting gypsum caves with microgravity and ERT under soil water content variations (Sorbas, SE Spain). Eng Geol.2015 Jul 2; 193:38–48.

McNeill J.D. and Labson V.F. 1991. Geological mapping using VLF radio fields. In: *Electromagnetic Methods in Applied Geophysics II* (ed. M.N. Nabighian), pp. 521–640. SEG.